frontiers | Frontiers in Energy Research

TYPE Original Research
PUBLISHED 30 May 2023
DOI 10.3389/fenrg.2023.1205840

OPEN ACCESS

EDITED BY
Xiaohuan Zhao,
Jinan University, China

REVIEWED BY
Yinjie Ma,
Hunan University, China
Jiaqiang E,
Hunan University, China

*CORRESPONDENCE
Ziheng Zhao,
221076846@stdmail.gxust.edu.cn

RECEIVED 14 April 2023
ACCEPTED 17 May 2023
PUBLISHED 30 May 2023

CITATION
Chen X, Jiang Y and Zhao Z (2023), Prediction of combustion and exhaust emissions of a CI engine fueled with diesel-biodiesel blends with different EGR rates.
Front. Energy Res. 11:1205840.
doi: 10.3389/fenrg.2023.1205840

Prediction of combustion and exhaust emissions of a CI engine fueled with diesel-biodiesel blends with different EGR rates

Xiaolong Chen[1], Yuxiu Jiang[1] and Ziheng Zhao[2]*

[1]School of Vehicle Engineering, Guangxi Vocational and Technical Institute of Industry, Nanning, China, [2]School of Mechanical and Automotive Engineering, Guangxi University of Science and Technology, Liuzhou, China

In this paper, the effects of diesel-biodiesel blends with different exhaust gas recirculation (EGR) rates on cylinder pressure, cylinder temperature, brake specific fuel consumption (BSFC), and brake thermal efficiency (BTE) of diesel engines are investigated. The emissions of nitrogen oxides (NO_x), carbon monoxide (CO), hydrocarbon (HC), and soot are also predicted to some extent. In this paper, a 3D-computational fluid dynamics (CFD) model of the in-cylinder combustion of a diesel engine is developed using the simulation software CONVERGE combined with an improved kinetic mechanism. A series of sub-models including the combustion, injection, and emission models are selected and presented, and the model's accuracy is verified based on experimental results. The results show that the cylinder pressure and in-cylinder temperature show a decreasing trend with an increasing EGR rate. In addition, BSFC increases with increasing EGR rate, and BTE decreases accordingly. When the EGR rate increased, the emission of NO_x decreased significantly, and the higher the EGR rate, the more obvious the decrease. The emission of soot, HC, and CO tended to increase with the increase of the EGR rate.

KEYWORDS

exhaust gas recirculation, diesel-biodiesel, combustion characteristic, emission improvements, renewable energy

1 Introduction

Since its introduction in the 1860s, the internal combustion engine has occupied an important place in the social development of mankind and has become a perfect machine after a century of continuous development and optimization (Cai et al., 2023; Hu et al., 2023). Although more and more new power systems are being proposed today, it is undeniable that the internal combustion engine will remain an important power unit for a long time to come (Zhang et al., 2022c; Huang et al., 2022). The use of internal combustion engines will consume a large amount of fossil fuels (Cui et al., 2023). The diesel engine, as one of the important representatives of the internal combustion engine, is widely used in automobiles, agricultural machinery, ships, etc. (Zhang et al., 2021; Yin et al., 2022). It has the advantages of high torque, high thermal efficiency, and good economic performance, but diesel engine emits relatively high Particulate matter (PM), Carbon dioxide (CO_2), and NO_x compared with gasoline engine (Zhang et al., 2022d), which is the main culprit of polluting the atmosphere and causing haze, acid rain, and the greenhouse effect (Tan et al., 2021; Zhang et al., 2023). In recent years, many countries around the world have started to pay attention

to the environmental pollution problem and set up strict emission regulations (Zhang et al., 2022; Zhang et al., 2023b). On one hand, in order to meet the increasingly stringent emission regulations and the deteriorating atmospheric environment, strict control measures on diesel exhaust emissions are needed (Tan et al., 2023b; Shi et al., 2023; Ye et al., 2023). On the other hand, in order to reduce the dependence on traditional fossil fuels and reduce emissions, biodiesel as an alternative fuel is gaining more and more attention from scholars (Zhao et al., 2022; Zuo et al., 2022). Biodiesel is a renewable and clean energy source, which can be extracted from animal fats, vegetable oils, and some household expenses from a wide range of sources (Zhang et al., 2022e; Zhao et al., 2023). Moreover, biodiesel is highly adaptable to diesel engines and can be used directly without structural modifications to diesel engines, which is the reason why it is so popular (Wu et al., 2022; Tan et al., 2023a).

Yilbasi et al. (2022) produced biodiesel from industrial hemp seed oil using a single-stage homogeneous catalytic transesterification process and tested the combustion and emission performance of this biodiesel and diesel blend. The results showed that although the thermal efficiency of biodiesel was slightly lower than that of diesel under load, the emissions of CO, HC, and soot were lower for biodiesel and its blends. Zhang et al. (2022b) investigated the performance of different generations of biodiesel diesel engine performance, combustion, and emissions. The results proved that the use of different generations of biodiesel reduced the engine CO emissions by 30%, HC emissions by 50%, and soot emissions by 70%.

Many scholarly studies have reported that the addition of additives to biodiesel-diesel blends is effective in reducing CO, HC, and particulate emissions (Palani et al., 2022). Devarajan et al. (2022) investigated the performance, emission, and combustion characteristics of n-butanol blended biodiesel at two ratios of 5% and 10%. The results of the experiments showed a significant reduction in CO, HC, and soot opacity emissions compared to standard diesel. Dhanarasu et al. (2022) studied the effect of nano-additions on the overall performance of biodiesel-diesel blends. The results showed that the addition of nanoparticles helped to reduce CO emissions due to the higher thermal conductivity and surface-to-volume ratio of nanoparticles. Also, there is a significant reduction in HC emissions because nanoparticles enhance the combustion of the fuel. Nanoparticles such as Ce_2O_3, Graphene Oxide (GO), and Carbon Nanotube (CNT) are effective in reducing NO_x emissions. The combustion and emission performance of biodiesel blends of diesel and glycine in diesel engines were studied by other scholars (Hua et al., 2022; Kumar et al., 2022; Shanmugam et al., 2022; Fayad et al., 2023). The results of the study showed that the NO_x emission of the blended diesel was higher than that of diesel, but there was a significant decrease in CO_2 emission. Chaitanya et al. (2022) studied the combustion and emission performance of a blend of ethanol, biodiesel, and diesel in a common rail diesel engine. The higher oxygen content of ethanol promoted the combustion process and improved thermal efficiency. In terms of emissions, the addition of ethanol reduced the soot emissions by 50% (Dineshkumar et al., 2022).

The above results showed that biodiesel has a significant reduction in CO, PM, and HC emissions compared to diesel due to the complete combustion with abundant oxygen content (Zhang et al., 2023c), but the NO_x emissions from biodiesel combustion are significantly higher than diesel, and how to reduce NO_x emissions has become a research direction for many scholars. EGR as an effective means to reduce NO_x emissions from biodiesel, has become a popular research subject (E et al., 2017). Li et al. (2014) investigated the NO_x emissions of biodiesel-diesel blends in light duty diesel engines. The experimental results showed that when the EGR increased from 19.6% to 25%, the NO_x emissions of 50 vol% biodiesel-50 vol% diesel and pure diesel were close to each other, and when the EGR was increased to 28%, the NO_x emissions were further reduced; Mamat et al. (2013) explored the effect of the EGR system at different temperatures on the exhaust gas emissions of inline four-cylinder diesel engines using biodiesel The effect of EGR on the exhaust gas emissions of inline four-cylinder diesel engines using biodiesel was investigated. The experimental results showed that there was a significant reduction in NO_x emissions in the engine with EGR, which was about 50% of that in the engine without EGR, but the emissions of CO and Total hydrocarbons (THC) were relatively high. Ramadhas et al. (2010) investigated the performance and emissions of a single-cylinder diesel engine fueled by a biodiesel-diesel blend with different EGR. The experimental results showed that the recirculation of exhaust gases lowered the temperature of the combustion chamber and an increase in thermal efficiency could be clearly observed and the engine with EGR had lower exhaust efficiency. Kim et al. (2020) investigated the emission characteristics of diesel and biodiesel compression ignition engines with different injector orifices and EGR conditions. The results showed that the NO_x emissions of the diesel engine with EGR were 50% of those of the diesel engine without EGR when the mixture of biodiesel and pure diesel was 20%, but there was no significant effect on the emissions of CO and CO_2. Chandravanshi et al. (2022) extensively studied the use of biodiesel-diesel blends and EGR in a four-stroke single-cylinder vertical diesel engine to obtain the best diesel engine performance and emission profile. His results showed that EGR can effectively reduce NO_x emissions, but when EGR reaches 30% it reduces the usage performance and brings more CO and HC emissions. To mitigate this situation, a combination of 5% ethanol and magnetized material at 10% EGR was used as a way to obtain the best performance. Esakki et al. (2022) investigated the net effect of EGR on combustion, performance, emission, and energy characteristics of common rail direct injection (CRDI) engines (Jayabal et al., 2022). The experimental results showed that BTE was slightly increased at lower EGR rates and HC emissions decreased by 85.71% and CO emissions decreased by 50% at B10 and EGR by 5% compared to diesel-only conditions. The effect of different EGR rates on the combustion and emission characteristics of diesel engines with biodiesel-diesel blends was investigated by Ramesh et al. (2022). The effects of different EGR rates on in-cylinder pressure, in-cylinder temperature, BSFC, BTE, NO_x emissions, HC emissions, CO emissions, and soot emissions were simulated and analyzed. The results of the study showed that the in-cylinder pressure and in-cylinder temperature decreased with increasing EGR. NO_x emissions reached the optimum reduction of 78.89% at 15% EGR, but CO, HC, and soot emissions increased with increasing EGR. Venu et al. (2019) conducted a study on the synergistic effect of biodiesel-diesel

TABLE 1 Main parameters of internal combustion engine.

Parameters	Value	Parameters	Value
Bore×stroke (mm)	190 × 210	Initial cylinder turbulence energy (m^2/s^2)	18.375
Connecting Rod (mm)	410	Compression ratio	14
Rated rpm (r/min)	1,000	Initial pressure at the air inlet (MPa)	0.193
Number of fuel injection holes	8	Effective power (kW)	220
Nozzle radius (mm)	0.28	Spraying angle (°)	150

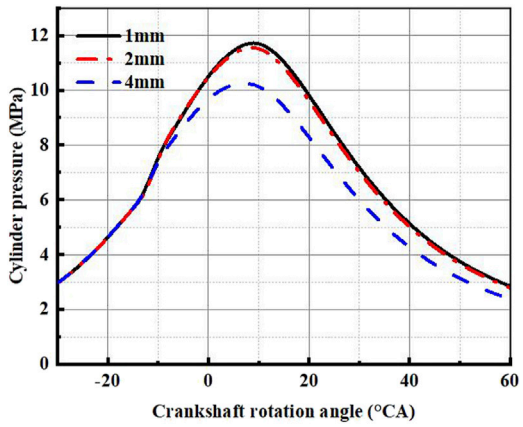

FIGURE 1
Cylinder pressure curves for three different grids.

blends, nanoparticles, and EGR (Bertinatto et al., 2022). The experimental test results illustrated that the HC, CO, and BSFC of the Palm Biodiesel Nanoparticles (PBN)-EGR system decreased significantly with increasing EGR compared to the conventional PBN-EGR system, and the NO_x emission of the PBN-EGR system was comparable to that of PBN-EGR in the experiment. Dubey et al. (2022) investigated the effects of biodiesel and n-pentanol on the emissions of a common rail diesel engine at different exhaust gas recirculation rates. The results of the test illustrated that B20P10 (20% biodiesel, 10% n-pentyl alcohol, and 70% diesel by volume) had the best combustion and emission performance (Liang et al., 2021; Krishnan and Rajkumar, 2022). This is mainly reflected in the significant reduction of soot and CO emissions of B10P20 at different EGR rates compared to pure diesel, especially at high EGR rates. Ozturk and Can (2022) investigated the effect of EGR, injection delay, and ethanol addition on the performance of Canola biodiesel-diesel blends. The experimental results proved that 5% EGR can effectively mitigate the combustion parameters of B10 biodiesel blends and delayed injection can effectively improve the emission parameters. In addition, all three methods can effectively reduce NO_x emissions.

In conclusion, biodiesel-diesel blends not only have the advantage of being renewable, but also can well improve the emission of pollutants such as CO, HC, and soot, but still have significant deficiencies in NO_x emissions. EGR technology brings environmentally beneficial emission reduction while improving engine fuel efficiency. Therefore, it is of great practical value to study the improvement of combustion and emission performance of engines with different EGR rates. In this paper, a 3D-CFD model is developed using CONVERGE software combined with the kinetic mechanism. The 3D-CFD model is based on a chemical reaction mechanism to describe the combustion process of fuel, which includes oxidation reaction of fuel, multiphase reaction during combustion, multiphase heat transfer, mass transfer, and phase change. This study has a theoretical reference value for reducing diesel engine pollution and provides a certain database and reference value for the subsequent research of diesel engine EGR control strategy.

2 Model building and validation

In this chapter, a 3D-CFD model is developed and experimentally validated using commercial simulation CONVERGE software combined with the chemical kinetic mechanism. The 3D-CFD model describes the combustion process of fuel based on the chemical reaction mechanism, which includes the oxidation reaction of fuel, multiphase reaction during combustion, multi-phase heat transfer, mass transfer, and phase change. It can effectively predict the combustion and emission conditions in diesel engines.

2.1 Numerical model

In the 3D-CFD model built using CONVERGE, the numerical model mainly consists of the mass conservation equation, the energy conservation equation, and the gas state equation (Zhao et al., 2021). Modifying the flow ratio and flow between the inlet and EGR airflow can control the oxygen content of the inlet and the exhaust gas content in the exhaust duct at different EGR rates, thus controlling the combustion and emission performance of the diesel engine. The adjustment of these variables can be controlled by the CONVERGE software.

2.1.1 Conservation of mass equation

Fluid mass conservation mainly means that the increase of mass in a fluid micro-element per unit of time is equal to the net mass flowing into that micro-element. In fluid computational mechanics, the continuity equation is a manifestation of fluid mass conservation. The mass conservation equation is as follows:

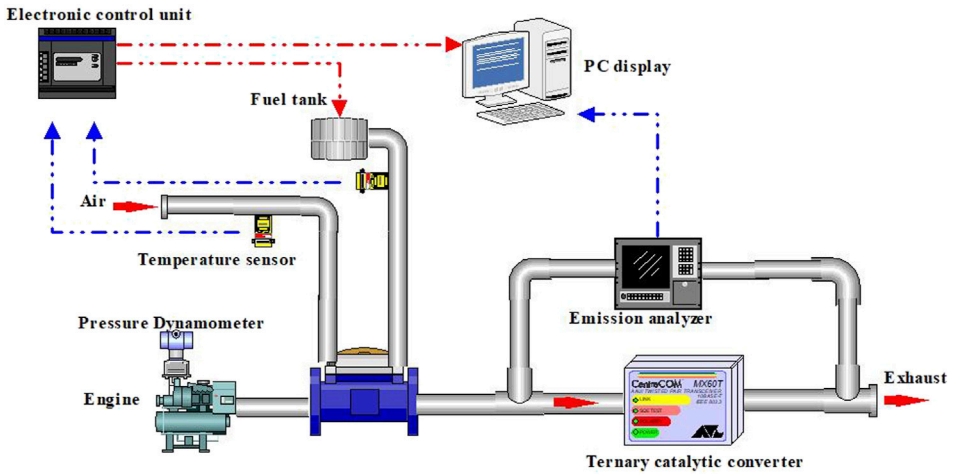

FIGURE 2
Experimental setup diagram.

TABLE 2 Measurement range, uncertainty, and accuracy of relevant parameters.

Parameters	Measuring range	Accuracy	Uncertainty
Pressure	0–25 MPa	±10 kPa	±0.55%
Engine speed	1–2000 rpm	±40 rpm	±0.24%
Crank angle encoder	0–720°CA	±0.5 °CA	±0.30%
BTE	—	±0.5%	±1.70%
BSFC	—	±5.10g/(KW·h)	±1.50%
NO_x emissions	0–6,000 ppm	±10 ppm	±0.54%
CO emission	0–12% vol	±0.04%	±0.33%

$$\frac{dm_A}{d\theta} = \sum \frac{dm_B}{d\theta} - \sum \frac{dm_D}{d\theta} - \frac{dm_E}{d\theta} + \frac{dm_C}{dt} \quad (1)$$

where, m_A is the sum of the mass of all substances in the cylinder, kg; θ is the crankshaft rotation angle, °CA; m_B is the mass of gas flowing into the cylinder, m_C is the mass of fuel flowing into the cylinder, kg; m_D is the mass of gas entering the cylinder, m_E is the mass of gas discharged from the cylinder, kg; t is the time, s.

2.1.2 Energy conservation equation

Based on the first law of thermodynamics, a flow system with heat exchange must satisfy the law of energy conservation, where the increment of energy in the micro-element is equal to the net heat of the micro-element plus the work done by the body force and the surface force.

The conservation of energy equation is as follows:

$$\frac{d(m_A \cdot u)}{d\theta} = -p_c \cdot \frac{dV}{d\theta} + \frac{dQ_F}{d\theta} - \sum \frac{dQ_W}{d\theta} - h_b \cdot \frac{dm_E}{d\theta} + \sum \frac{dm_B}{d\theta} \cdot h_i - \sum \frac{dm_D}{d\theta} \cdot h_a - q_e \cdot f \cdot \frac{dm_C}{dt} \quad (2)$$

where, u for the cylinder-specific internal energy, J/kg; p_c for the cylinder pressure, Pa; V for the work volume, cm^3; Q_F for the fuel heat release, J; Q_w for the heat loss, J; h_a for the specific enthalpy of outflow gas, J/kg; h_b for the specific enthalpy of leakage gas, J/kg; h_i for the specific enthalpy of inflow gas, J/kg; q_e for the latent heat of evaporation of fuel, J; f for the mass fraction of evaporated fuel.

2.1.3 Ideal gas equation of state

The gas equation of state reflects the relationship between the temperature, density, and pressure of a gas.

The ideal gas equation of state is as follows:

$$p_c = \frac{1}{v} \cdot m_A \cdot R_c \cdot T_c \quad (3)$$

where R_c is the gas constant, J/(K·kg); T_c is the cylinder body temperature, K.

2.1.4 Component transport equation

The law of conservation of components means that the rate of change of the mass of the chemical components within the system with respect to time is equal to the sum of the production rate of the components generated through the chemical reaction and the net diffusive flow through the system cross-section.

The component transport equations are as follows:

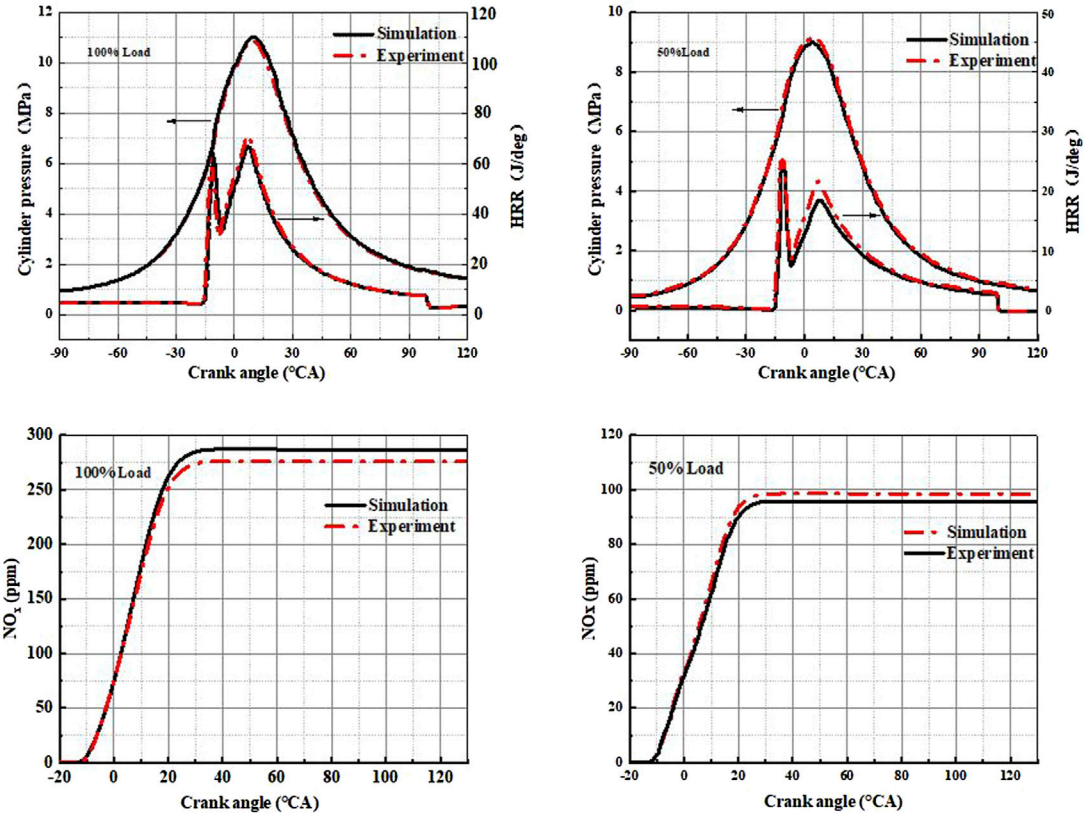

FIGURE 3
Experimental and simulated NO_x emission trend under 100% and 50% load conditions.

$$\frac{\partial \rho_m}{\partial t} + \frac{\partial p_m u_1}{\partial x_i} = \frac{\partial}{\partial x_i}\left(\rho D \frac{\partial Y_i}{\partial x_i}\right) + S_m \tag{4}$$

$$Y_m = \frac{N_m}{N_{tt}} = \frac{\rho_m}{\rho_{tt}} \tag{5}$$

where, ρ is the fluid density, kg/m^3; u_1 is the velocity vector, m/s; D is the mass diffusion coefficient, m^2/s; Y_i is the mass fraction of component m, %; S_m denotes the generation rate of component m per unit time. N_m is the mass of the micro-element control body component m, kg; N_{tt} is the total mass of the micro-element control body component, kg.

2.2 Jet model

The fuel injection process is often influenced by parameters such as the aperture of the injection hole, the ambient pressure at the time of injection, and the injection pattern (Wei et al., 2019). In this study, Kelvin-Helmholtz & Rayleigh-Taylor (KH-RT) was used as the crushing model (Rostampour et al., 2022), the Frossling model to obtain the rate of change of fuel droplet size, and also the dynamic droplet drag model was used to determine the gas drag.

Where KH-RT is determined by the following equation:

$$R_A = C_a \Lambda \tag{6}$$

$$\tau = \frac{3.7 C_1 r_A}{\Lambda \Omega} \tag{7}$$

$$\Lambda = \frac{9.02 r_A \left(1 + 0.45 O_H^{0.5}\right)\left(1 + 0.4 T_{KH}^{0.7}\right)}{\left(1 + 0.865 {W_e}^{1.67}\right)^{0.6}} \tag{8}$$

$$\Omega = \frac{0.34 + 0.38 {W_e}^{1.5}}{\left(1 + O_a\right)\left(1 + 0.4 T_{KH}^{0.6}\right)} \sqrt{\frac{\sigma}{\rho l r_A^3}} \tag{9}$$

where R_A is the initial radius, m; C_a and C_1 are the injector constants; Λ is the wavelength, m; Ω is the wave height index; τ is the oil beam presence time, s; r_A is the droplet radius, m; W_e is the Weber number of the continuous phase; O_a is the Anseger number of the droplet; σ is the surface tension; T_{KH} is the Taylor number; ρ_l is the density of the liquid, kg/m^3.

2.3 Turbulence model

The turbulence model for this study uses the Reorganization group (RNG) k-ε model (Analytis, 2003).

Where kinetic energy k and dissipation rate ε obtained from the following equations:

$$\frac{\partial \rho_k}{\partial t} + \frac{\partial \left(\rho u_i k\right)}{\partial x_i} = \tau_{ij} \frac{\partial u_i}{\partial x_i} + \frac{\partial}{\partial x_j}\left(\frac{\mu_e}{Pr_k} \frac{\partial k}{\partial x_j}\right) - \rho \varepsilon + S_a \tag{10}$$

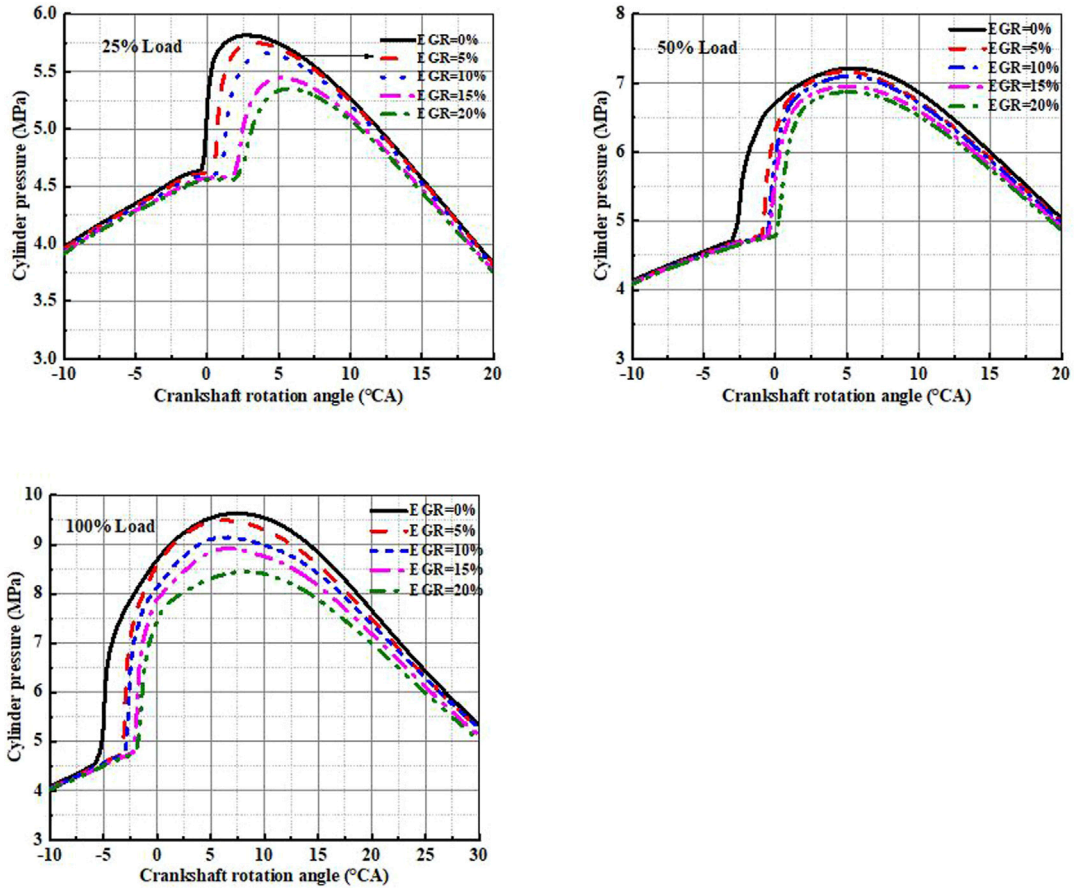

FIGURE 4
Comparison of cylinder pressure curves at different EGR rates.

$$\frac{\partial \rho_\varepsilon}{\partial t}+\frac{\partial(\rho u_i \varepsilon)}{\partial x_i}=\frac{\partial}{\partial x_j}\left(\frac{\mu_e}{Pr_\varepsilon}\frac{\partial k}{\partial x_j}\right)-C_{\varepsilon a}\rho\varepsilon\frac{\partial u_i}{\partial x_i}+\left(C_{\varepsilon b}\frac{\partial u_i}{\partial x_j}\tau_{ij}-C_{Sa}\rho\varepsilon+\varepsilon C_s S_a\right)\frac{\varepsilon}{k}+S-\rho R \quad (11)$$

where μ_e is the effective viscosity, Pa·s; Pr_k is the Prandtl number in the k-equation; Pr_ε is the Prandtl number in the ε-equation; τ_{ij} is the Reynolds stress, Pa; S_a represents the source term; $C_{\varepsilon a}$, $C_{\varepsilon b}$, and C_s are empirical constants.

2.4 Combustion model

In this paper, the SAGE model, which is more accurate in terms of chemical kinetics, is used to simulate the combustion conditions inside a diesel engine (Li et al., 2019). The diesel/biodiesel mechanism used in this paper is the biodiesel mechanism from Hunan University (E et al., 2016). Firstly, a detailed biodiesel combustion mechanism was abstracted and the relevant reaction paths were simplified by the DRGEPSA method; then the four methods of peak concentration analysis, isomer induction, non-significant reaction elimination, and reaction rate adjustment were combined to gradually eliminate the unimportant reactants and chemical reactions and reduce to obtain the final simplified combustion mechanism; finally, a three-component simplified combustion mechanism was coupled and the reaction rate adjustment was performed to obtain the desired simplified combustion mechanism. Finally, a three-component simplified combustion mechanism was coupled with a three-component simplified combustion mechanism with reaction rate adjustment to obtain the desired simplified combustion mechanism, which contained 106 reactants and 263 chemical reactions. In order to verify the applicability of the combustion mechanism, the original combustion mechanism ignition delay verification, reflective excitation tube ignition delay verificatio n, and diesel engine experimental verification were performed. The results showed that the combustion mechanism can simulate the ignition behavior of the components in the original detailed combustion mechanism and can predict the cylinder pressure, heat release rate, and NO_x emission of biodiesel with different fatty acid methyl ester ratios in the diesel engine.

The specific multi-step reactions are shown below:

$$\sum_{n=1}^{N} v'_{n,r} x_n \leftrightarrow \sum_{n=1}^{N} v''_{n,r} x_n \quad (r = 1, 2, ...N) \quad (12)$$

$$\dot{\omega} = \sum_{r=1}^{R} v_{n,r} q_r \quad (n = 1, 2, ...R) \quad (13)$$

$$v''_{n,r} - v'_{n,r} = v_{n,r} \quad (14)$$

$$q_r = k_{fr} \prod_{n=1}^{N} [X_n]^{v'_{n,r}} - k_{rr} \prod_{n=1}^{N} [X_n]^{v''_{n,r}} \quad (15)$$

where N is the total number of substances; $v'_{n,r}$ and $v''_{n,r}$ are the stoichiometric coefficients of reactants and products of component

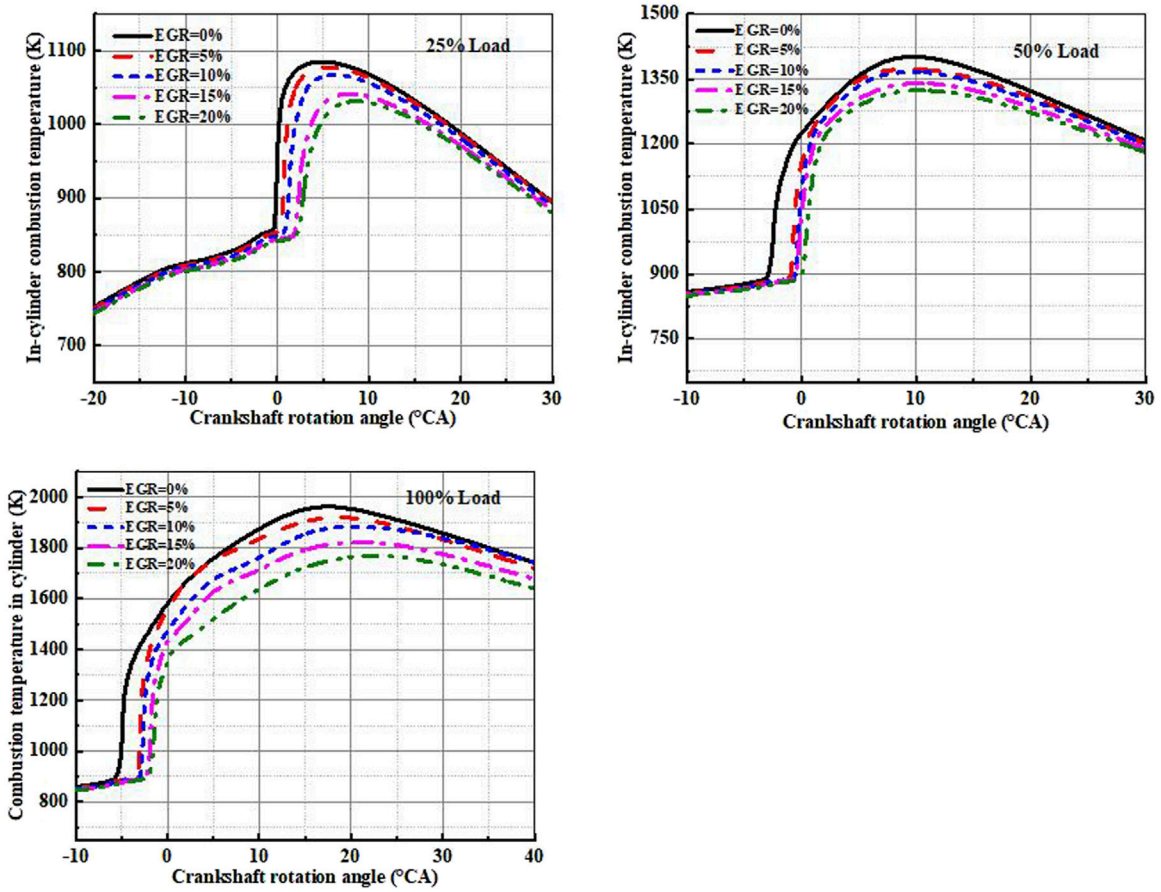

FIGURE 5
Comparison of cylinder temperature curves at different EGR rates.

n and reaction r, respectively; R is the total number of reactions; x_n is the chemical symbol of component n; k_{fr} and k_{rr} are the forward and reverse reaction rate coefficients of reaction r; $[X_n]$ is the molar concentration of substance n.

2.5 Heat transfer model

In this paper, the Amsden model and the O′Rourke model are used as the heat transfer models for the study (Duan et al., 2017).

The heat exchange model is calculated as follows:

$$k\frac{\mathrm{d}T}{\mathrm{d}x_i}=\begin{cases}\dfrac{\mu c_p\left(T_b-T_a\right)}{yPr_t n_i} & y^+<11.05\\ \dfrac{\rho c_p \mu_\tau T_b \mathrm{In}\left(\dfrac{T_b}{Ta}\right)n_i}{2.1\mathrm{In}\left(y^+\right)+2.513} & y^+>11.05\end{cases} \tag{16}$$

where Pr_t is the molecular Prandtl number; k is the molecular conductivity coefficient; T_a is the fluid temperature, K; T_b is the wall temperature, K; μ_τ is the shear velocity, μm/s; y^+ is the dimensionless distance, m.

2.6 Emission model

The present study used the extended Zeldovich NO_x model as an emission model (Yousefi et al., 2018).

The main reaction equations are shown below:

$$O_2 \leftrightarrow 2O \tag{R1}$$
$$O_2 + N \leftrightarrow O + NO \tag{R2}$$
$$N_2 + O \leftrightarrow O + NO \tag{R3}$$
$$N + OH \leftrightarrow NO + H \tag{R4}$$

2.7 Experimental protocol and experimental validation

2.7.1 Diesel engine main parameters and boundary conditions

The temperature boundary conditions are given empirically with the following relevant settings: piston temperature is 553 K, cylinder head temperature is 523 K, cylinder wall temperature is 373 K, and injector nozzle temperature is 550 K. Velocity boundary

TABLE 3 Diesel engine in-cylinder combustion temperature field distribution.

Loads	ATDC	EGR = 0%	EGR = 5%	EGR = 10%	EGR = 15%	EGR = 20%	Color scale
100% Load	ATDC = 0°CA	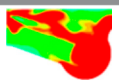	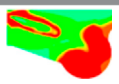	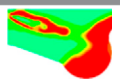	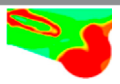	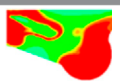	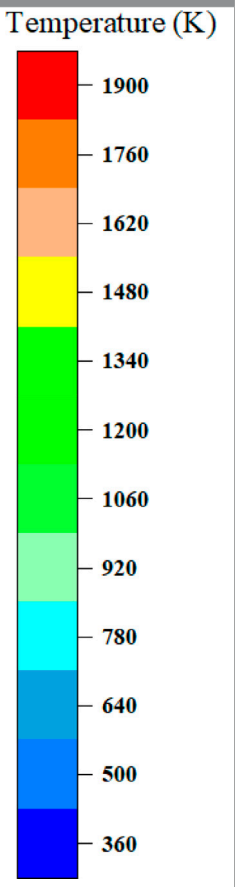
	ATDC = 10°CA	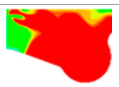	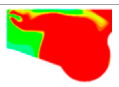	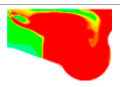	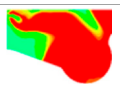	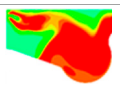	
50% Load	ATDC = 0°CA	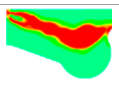	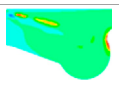	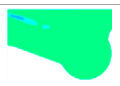	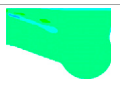	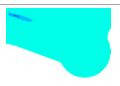	
	ATDC = 10°CA	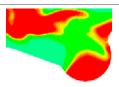	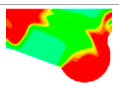	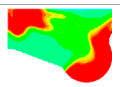	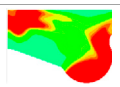	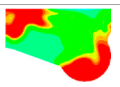	
25% Load	ATDC = 0°CA						
	ATDC = 10°CA	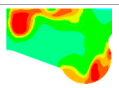	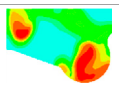	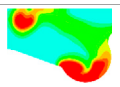	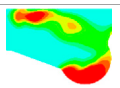	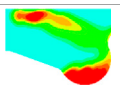	

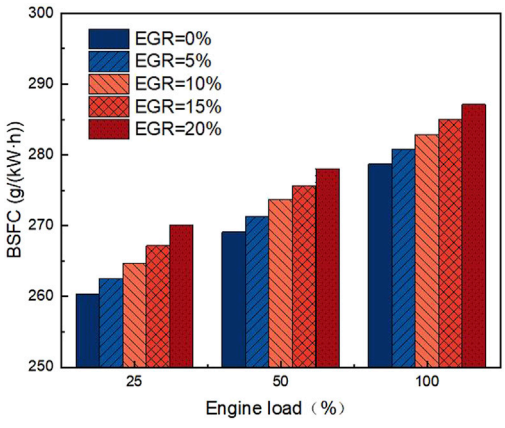

FIGURE 6
The effect of EGR rate on engine BSFC at different loads.

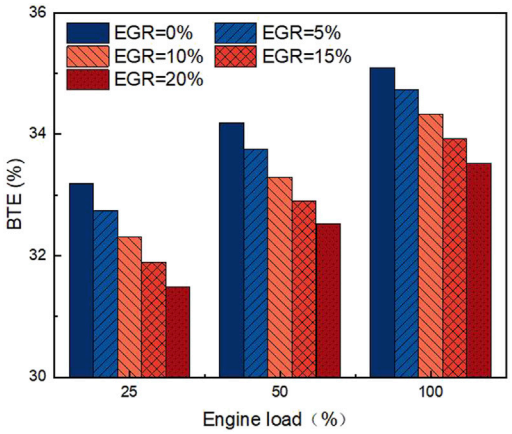

FIGURE 7
The effect of EGR rate on engine BTE at different loads.

conditions: the piston motion speed is the actual piston movement speed at the calculated speed, and the rest of the components are stationary.

The Turbulent Kinetic Energy (TKE) and Turbulence Length Scale (TLS) in the initial combustion chamber are calculated by the following equations:

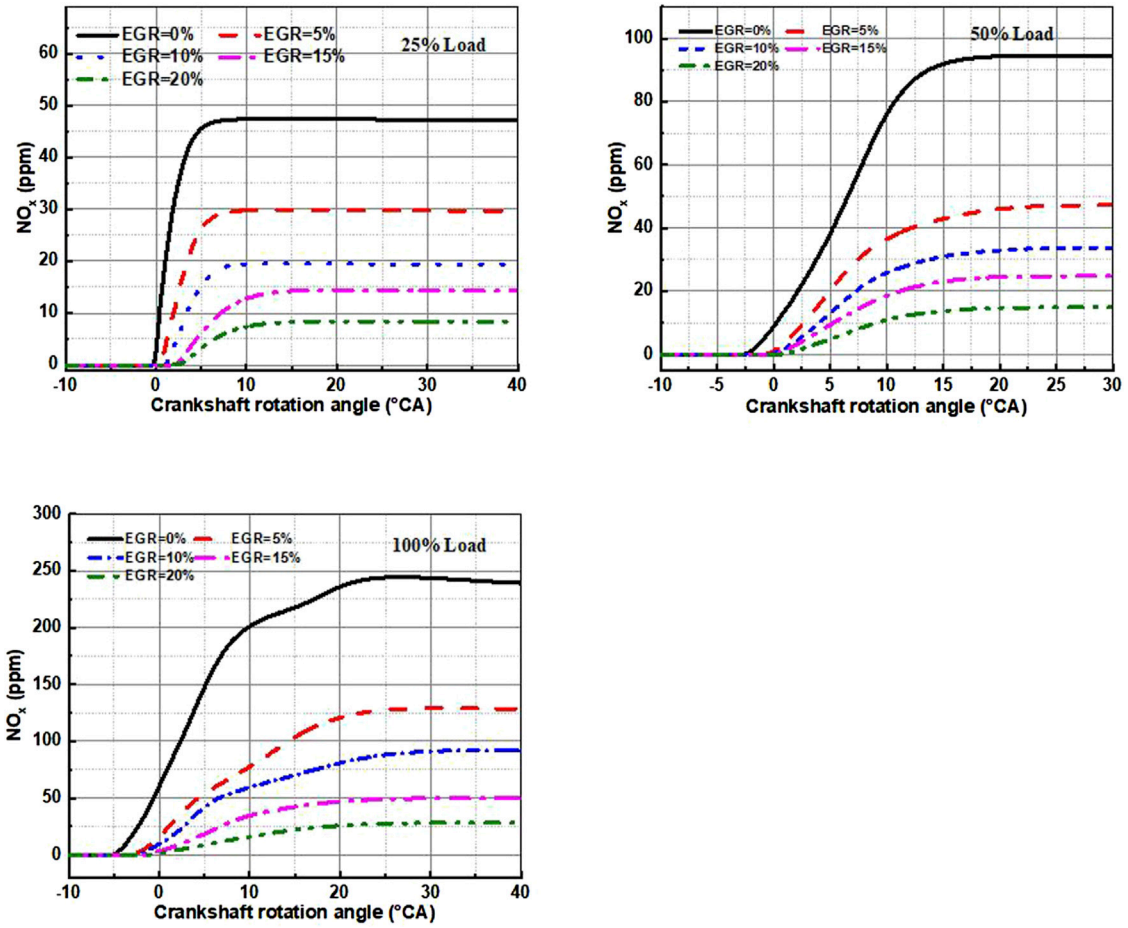

FIGURE 8
Comparison of NO_x emission profiles at different EGR rates.

$$TKE = \frac{3}{2} \times u_2 \tag{17}$$

$$u = 0.7 \times 2 \times h \times \frac{n}{60} \tag{18}$$

$$TLS = \frac{h_v}{2} \tag{19}$$

where, u_2 indicates turbulent pulsation velocity, mm/s; h is the diesel engine stroke, mm; n is the diesel engine speed, rpm; h_v is the maximum valve lift, mm.

The main parameters of the diesel engine are shown in Table 1.

2.7.2 Grid independence verification

Generally speaking, the finer the grid the more accurate the prediction made by the model. Figure 1 shows the pressure transformation curves of the cylinder when the grids are 1mm, 2mm and 4 mm respectively. At the upper stop, the number of meshes of the three meshes are 463,250, 375,500, and 286,300, and the time spent is 15, 10, and 7 h respectively. 2 mm mesh has the same accuracy as 1 mm, and the calculation time is shorter, so 2 mm mesh is used for simulation.

2.7.3 Feasibility test

In this paper, a 3D-CFD model of a diesel engine was developed using CONVERGE software to study the combustion performance and emission performance of diesel-biodiesel blends at different EGR rates and under different loads. The setup of the experiment is shown in Figure 2. The Horiba MEXA1600 was mainly used to test the NO_x emissions. Soot emissions were measured by AVL Dismoke-4000. FCMM-2 and DEWE-2010CA were used to monitor diesel engine BSFC and combustion, respectively. The fuel rate was measured using EFS-IFR600. Diesel engine loads were measured by a hydraulic dynamometer. In addition, engine power, pressure, temperature, and flow were measured by a Xiang Yi eddy current dynamometer and the corresponding sensors. Table 2 shows the measurement ranges and error margins of these instruments. In addition, to ensure the stability of the measurements, the experimental results were recorded three times for averaging after 25 min of smooth operation of the diesel engine.

2.7.4 Model validation

In this section, the accuracy of the simulation model is tested. The experimental results and the model simulation results were

TABLE 4 NO_x distribution field in the cylinder.

Loads	ATDC	EGR = 0%	EGR = 5%	EGR = 10%	EGR = 15%	EGR = 20%	Color scale
100% Load	ATDC = 0°CA	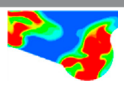	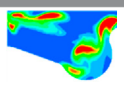	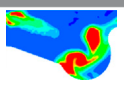	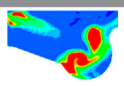	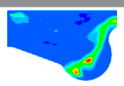	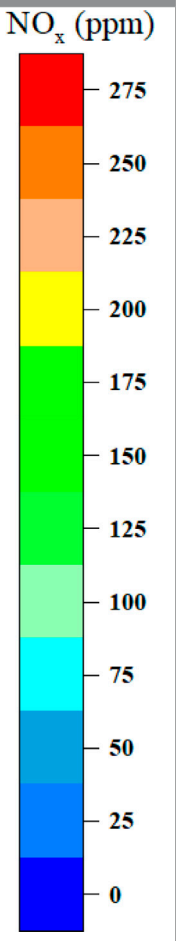
	ATDC = 10°CA	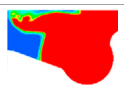	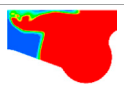	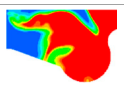	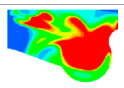	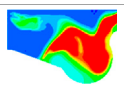	
50% Load	ATDC = 0°CA	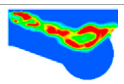					
	ATDC = 10°CA	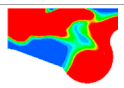	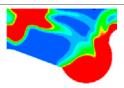	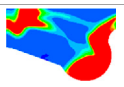	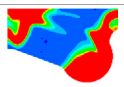	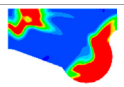	
25% Load`	ATDC = 0°CA						
	ATDC = 10°CA	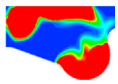	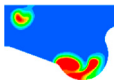	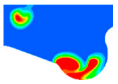	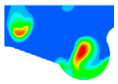	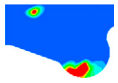	

compared at 100% and 50% loads, respectively. As shown in Figure 3, the errors are within 5%, and the simulation results of the model can be trusted. Moreover, the experimental data and the simulated data match very well in terms of NO_x emission trends. So, the combustion and emission performance predictions using the model are accurate.

3 Results and discussion

3.1 Combustion characteristics

The combustion performance of a diesel engine changes to varying degrees with the EGR rate. This section shows in detail the changes in combustion pressure, combustion temperature, BSFC, and BTE in diesel engine cylinders at different EGR rates.

3.1.1 In-cylinder combustion pressure

Figure 4 shows the variation of cylinder pressure at different EGR rates. It can be clearly seen that when the EGR increases from 0% to 20%, the cylinder pressure shows a trend of decreasing step by step. The reason for this situation is that when the EGR rate is higher, the oxygen concentration in the cylinder is lower, which slows down the combustion of the fuel. The increase in fuel stagnation and combustion time is not conducive to fuel evaporation and atomization, so the end result shows a decrease in cylinder pressure.

3.1.2 In-cylinder combustion temperature

Figure 5 shows the variation of in-cylinder combustion temperature at different EGR rates. It can be seen that the in-cylinder combustion temperature has a clear tendency to decrease with the increase of EGR rate. For example, when the EGR rate rises from 0% to 5%, a decrease in combustion temperature can be seen significantly at 100% load, 50% load, and 25% load. This is because more exhaust gases enter the cylinder and the oxygen concentration decreases leading to deterioration of combustion. In addition, the increase in exhaust gas leads to an increase in the specific heat capacity of the gas in the cylinder, which also leads to a decrease in the in-cylinder combustion temperature.

Table 3 shows the temperature field distribution in the cylinder. It can be seen that as the EGR rate increases, the high-temperature region in the cylinder is gradually decreasing. In addition, as the

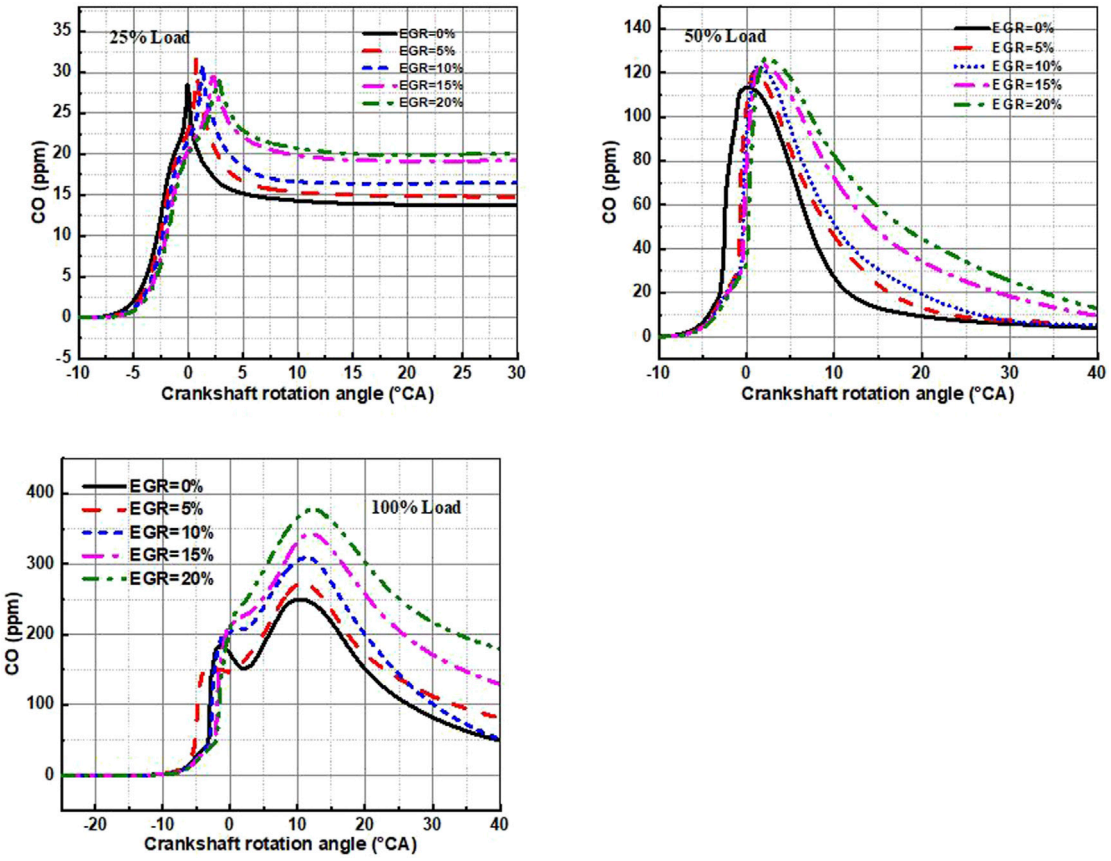

FIGURE 9
Comparison of CO emission profiles at different EGR rates.

EGR rate increases the oxygen concentration in the cylinder decreases, the combustion deteriorates, the combustion rate decreases, and the maximum burst pressure and maximum average temperature decrease. The introduction of EGR also brings about an extension of the stall period and pushes back the combustion start point, so that the crankshaft rotation angle corresponding to the maximum average combustion temperature also shifts back.

3.1.3 Brake specific fuel consumption

Figure 6 shows the positive relationship between the amount of BSFC and the EGR rate of the engine. For example, at 50% load, the BSFC increases by 0.83%, 1.72%, 2.43%, and 3.31% when the EGR rate is increased to 5%, 10%, 15%, and 20%, respectively. This is because increasing the EGR rate causes excess exhaust gases to enter the cylinders, and the decrease in oxygen concentration leads to a deterioration of the combustion process, which requires more fuel to be consumed to maintain performance.

3.1.4 Brake thermal efficiency

The economy of the engine can be demonstrated by the BTE. Figure 7 shows the trend of diesel engine BTE at different EGR rates. It is clearly seen that the BTE shows a decreasing trend with increasing EGR at all loads. The highest BTE is observed at 0% EGR. As the EGR increases to 5%, 10%, 15%, and 20%, the BTE decreases by 1.26%, 2.62%, 3.75%, and 4.87%, respectively. The reason for this trend is that the increase in EGR rate leads to a decrease in oxygen concentration and combustion temperature, which severely deteriorates the combustion process. In addition, the increase in EGR rate decreased the combustion time, which led to a decrease in the combustion rate and eventually led to a loss in thermal efficiency.

3.2 Emission characteristics

The various emission performance of diesel engine also changes to a different extent with the change in EGR rate. This section shows in detail the variation of diesel engine NO_x, CO, soot, and HC emissions at different EGR rates.

3.2.1 NO_x emissions

Compared to pure diesel, biodiesel-diesel blends emit more NO_x, and EGR is a means to effectively reduce NO_x emissions. As shown in Figure 8, the study results showed that at 100% load, NO_x emissions were reduced by 49.9%, 64.3%, 73.9%, and 84.3%

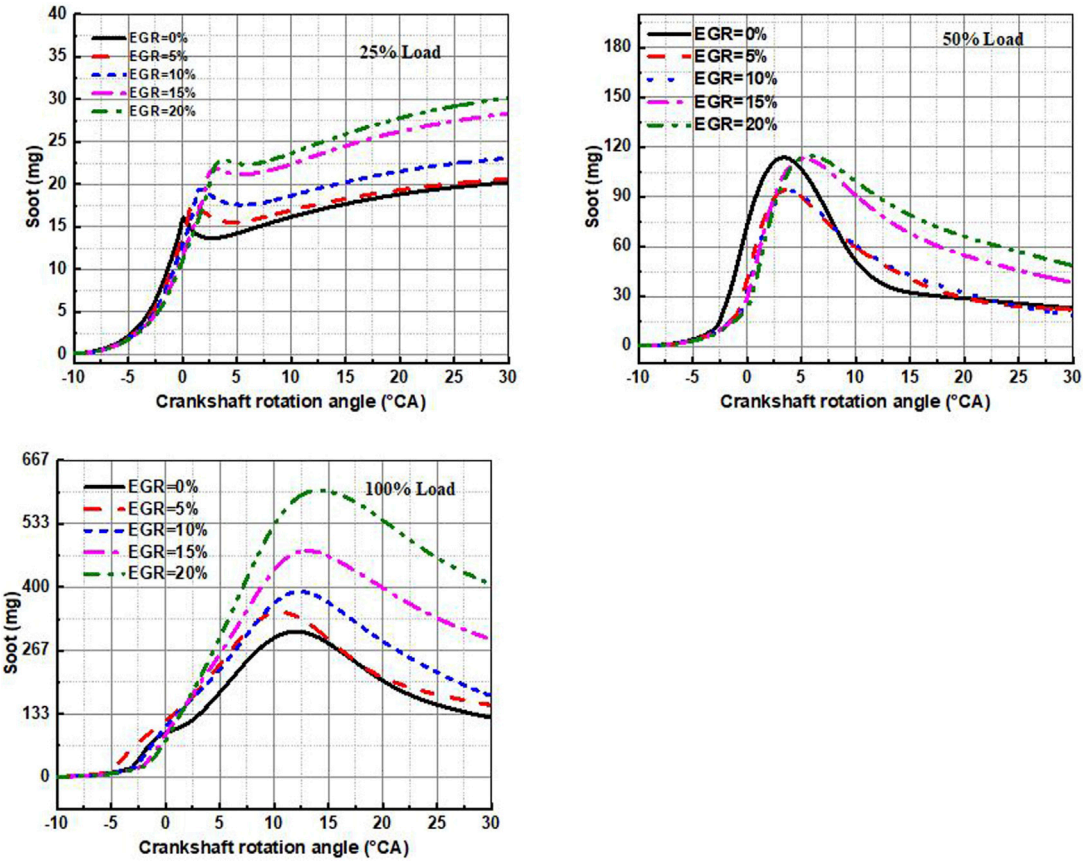

FIGURE 10
Comparison of soot emission curves at different EGR rates.

when EGR was increased to 5%, 10%, 15%, and 20%, respectively. This is because, on the one hand, the introduction of EGR makes the intake air flow lower, the actual excess air coefficient decreases the in-cylinder oxygen concentration, which destroys the NO_x generation conditions and NO_x emission decreases. On the other hand, the tri-atomic molecules such as CO_2 and water vapor enter the cylinder in EGR, which increases the specific heat capacity of the in-cylinder mass and reduces the maximum combustion temperature and pressure in the cylinder, which decreases the NO_x generation and therefore reduces the NO_x emission.

From Table 4 below, it can be seen that the distribution area of NO_x in the cylinder shows a trend of decreasing when the EGR rate increases. Combined with Table 3, it can be found that the distribution area of NO_x receives the influence of the temperature in the cylinder, and NO_x is more likely to be generated in the high-temperature area.

3.2.2 CO emission

Figure 9 shows the variation pattern of CO emissions with the EGR rate. It is clear that the higher the EGR rate is, the higher the CO emissions are. For example, at 100% load, the CO emission is 12.16% higher when the EGR rate is 20% than when the EGR rate is 0%. This is because the inert gas in the exhaust gas dilutes the oxygen concentration, and the increase in the oxygen-deficient area in the cylinder leads to an increase in the CO generated. In addition, the high specific heat capacity gases in the exhaust gas such as CO_2 and H_2O increase the specific heat capacity of the mixture, preventing the combustion reaction and reducing the maximum temperature in the cylinder. The reduced oxygen content and temperature in the cylinder make it difficult to oxidize the generated CO to CO_2, which eventually leads to an increase in CO emissions.

3.2.3 Soot emissions

Figure 10 shows the relationship between soot emissions and EGR rate. It can be seen that the increase in EGR rate obviously leads to an increase of soot emissions. When the load is 100% and the EGR rate is 20%, the soot emissions reach a maximum, emitting 49.2% more soot than a 0% EGR rate. Similar to CO, this is because the increasing EGR rate leads to a continuous reduction of the oxygen content in the cylinder, which does not allow sufficient combustion of the fuel and thus inhibits the oxidation of soot. In addition, the continuous reduction of oxygen content inhibits the oxidation of soot, which is also the reason for the increase in soot emissions.

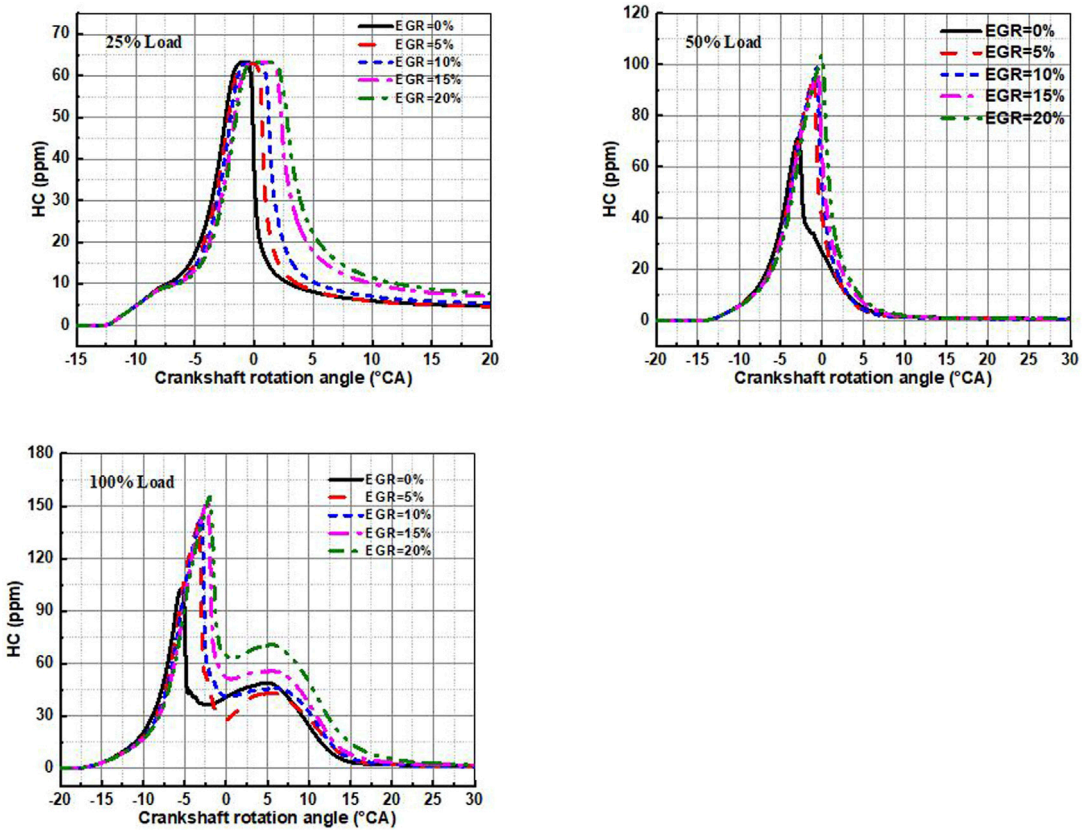

FIGURE 11
Comparison of HC emission curves at different EGR rates.

3.2.4 HC emissions

Figure 11 shows the relationship curve between HC emissions and EGR rate. It is clear that HC emissions increase with the increase in EGR rate. HC emissions reach their maximum when the EGR rate is 20%. Similar to soot, this is due to the increase in the EGR rate leading to a decrease in the oxygen concentration in the cylinder. The fuel does not get fully burned and the oxidation of HC is inhibited, resulting in higher HC emissions. In addition, the continuous increase in EGR rate leads to a decreasing combustion temperature in the cylinder. The quenching phenomenon in the cylinder is enhanced, and therefore the HC emissions are further increased.

4 Conclusion

In this study, by combining CONVERGE with an improved kinetic mechanism, a 3D-CFD model was established to analyze the improvement of in-cylinder pressure, in-cylinder temperature, fuel consumption, BTE, NO_x emission, CO emission, soot emission, and HC emission at different EGR rates. This paper has unique advantages in optimizing diesel engine combustion performance and reducing pollution emissions. This study provides some data support for subsequent EGR control studies, and the specific conclusions obtained are as follows:

(1) The increase of EGR leads to more exhaust gas flowing into the cylinder, which in turn reduces the oxygen concentration in the cylinder, ultimately leading to an increase in fuel consumption and a significant decrease in cylinder pressure, cylinder temperature, and BTE. At 50% load, as EGR increased from 0% to 20% in 5% increments each time, the values of BSFC increased by 0.83%, 1.72%, 2.43%, and 3.31%, respectively; and BTE decreased by 1.26%, 2.62%, 3.75%, and 4.87%, respectively.
(2) EGR can effectively reduce NO_x emissions, which are reduced by 84.3% at an EGR rate of 20%. This is due to the lower oxygen concentration and cylinder temperature suppressing NO_x production. Too high EGR rates instead bring an increase in HC, CO, and soot emissions. So, for the economic model, an EGR rate of about 15% is the best.

The above conclusion shows that the effect of the EGR rate on diesel engine is mainly due to the low oxygen concentration caused by the high EGR rate. And alcohol is rich in oxygen, so trying to add alcohol to the fuel mixture to obtain better combustion and emission performance is a potential way to reduce diesel engine emissions. In addition, the development of new materials and technologies to improve the durability and reliability of EGR systems will continue to be needed for future practical applications.

Data availability statement

The original contributions presented in the study are included in the article/supplementary material, further inquiries can be directed to the corresponding author.

Author contributions

XC: method, funding acquisition, conceptualization, writing—review and editing; YJ: resources, project administration, method, software, data curation, writing—original draft, writing—review and editing; ZZ: data curation, writing—review and editing. All authors contributed to the article and approved the submitted version.

Funding

This work is supported by the Guangxi Basic Ability Improving Programs of 2020KY39008 and the Key Scientific Research Projects of Guangxi Vocational and Technical Institute of Industry (2019015KY025), the work is also supported by the Guangxi Vocational Education Teaching Reform Research Project (GXGZJG2022B033).

Conflict of interest

The authors declare that the research was conducted in the absence of any commercial or financial relationships that could be construed as a potential conflict of interest.

Publisher's note

All claims expressed in this article are solely those of the authors and do not necessarily represent those of their affiliated organizations, or those of the publisher, the editors and the reviewers. Any product that may be evaluated in this article, or claim that may be made by its manufacturer, is not guaranteed or endorsed by the publisher.

References

Analytis, G. T. (2003). Implementation of the renormalization group (RNG) k–ε turbulence model in Gothic/6.lb: Solution methods and assessment. *Ann. Nucl. ENERGY* 30 (3), 349–387. doi:10.1016/S0306-4549(02)00061-0

Bertinatto, R., Schlosser, J. F., Herzog, D., Bertollo, G. M., Dal Mas, G., and Osmari, J. G. (2022). Gas emissions from an agricultural compression-ignition engine using Diesel, biodiesel and ethanol blends. *Cienc. Rural.* 52 (8), e20210210. doi:10.1590/0103-8478cr20210210

Cai, L., E, J., Li, J., Ding, J., and Luo, B. (2023). A comprehensive review on combustion stabilization technologies of micro/meso-scale combustors for micro thermophotovoltaic systems: Thermal, emission, and energy conversion. *Fuel* 335, 126660. doi:10.1016/j.fuel.2022.126660

Chaitanya, A. V. K., and Mohanty, D. K. (2022). Experimental investigation on the combustion, performance and emission characteristics of 1-pentanol blended waste plastic oil in a CRDI engine with EGR. *Energy* 256, 124574. doi:10.1016/j.energy.2022.124574

Chandravanshi, A., Pandey, S., and Malviya, R. K. (2022). Experimental investigation on the effects of using ethanol with biodiesel and diesel blends along with exhaust gas recirculation and magnetization of fuel in the diesel engine. *Environ. Prog. Sustain. Energy* 41 (5), e13844. doi:10.1002/ep.13844

Cui, S., Pang, S., Pang, D., Tian, F., and Yu, Y. (2023). The microstructure and pitting corrosion behavior of K-tig welded joints of the UNS S32101 duplex stainless steel. *MATERIALS* 16 (1), 250. doi:10.3390/ma16010250

Devarajan, Y., Munuswamy, D. B., Nalla, B. T., Choubey, G., Mishra, R., and Vellaiyan, S. (2022). Experimental analysis of Sterculia foetida biodiesel and butanol blends as a renewable and eco-friendly fuel. *Ind. Crops Prod.* 178, 114612. doi:10.1016/j.indcrop.2022.114612

Dhanarasu, M., Kumar, K. A. R., and Maadeswaran, P. (2022). Recent trends in role of nanoadditives with diesel-biodiesel blend on performance, combustion and emission in diesel engine: A review. *Int. J. Thermophys.* 43 (11), 171. doi:10.1007/s10765-022-03092-z

Dineshkumar, C., Jeyakumar, P. D., Pandian, C. K. A., Rajmohan, N., Elumalai, P. V., Kamesh, N., et al. (2022). Assessment on performance and emission characteristics of the CRDI engine fueled with ethanol/diesel blends in addition to EGR. *Int. J. Chem. Eng.* 2022, 4413617. doi:10.1155/2022/4413617

Duan, J., Liu, F., Yang, Z., Sun, B., Chen, W., and Wang, L. (2017). Study on the NO_x emissions mechanism of an NICE under high load. *Int. J. Hydrogen Energy* 42 (34), 22027–22035. doi:10.1016/j.ijhydene.2017.07.048

Dubey, A., Prasad, R. S., Singh, J. K., and Nayyar, A. (2022). Response surface methodology (RSM) based experimental and model analysis of diethyl ether-biodiesel-diesel blends with exhaust gas recirculation (EGR) on stationary diesel engine. *Pet. Sci. Technol.* 41 (12), 1272–1291. doi:10.1080/10916466.2022.2092136

E, J., Liu, T., Yang, W., Li, J., Gong, J., and Deng, Y. (2016). Effects of fatty acid methyl esters proportion on combustion and emission characteristics of a biodiesel fueled diesel engine. *Energy Convers. manage.* 117, 410–419. doi:10.1016/j.enconman.2016.03.021

E, J., Minhhieu, P., Zhao, D., Deng, Y., DucHieu, L., Zuo, W., et al. (2017). Effect of different technologies on combustion and emissions of the diesel engine fueled with biodiesel: A review. *Renew. Sust. ENERG Rev.* 80, 620–647. doi:10.1016/j.rser.2017.05.250

Esakki, T., Rangaswamy, S. M., and Jayabal, R. (2022). An experimental study on biodiesel production and impact of EGR in a CRDI diesel engine propelled with leather industry waste fat biodiesel. *Fuel* 321, 123995. doi:10.1016/j.fuel.2022.123995

Fayad, M. A., Ibrahim, S. I., Omran, S. H., Martos, F. J., Badawy, T., Al Jubori, A. M., et al. (2023). Experimental effect of CuO_2 nanoparticles into the RME and EGR rates on NO_x and morphological characteristics of soot nanoparticles. *Fuel* 331, 125549. doi:10.1016/j.fuel.2022.125549

Hu, W., E, J., Leng, E., Zhang, F., Chen, J., and Ma, Y. (2023). Investigation on harvesting characteristics of convective wind energy from vehicle driving on multi-lane highway. *Energy* 263, 126062. doi:10.1016/j.energy.2022.126062

Hua, Y., Wang, Z., Li, R., Liu, S., Zhao, Y., Qu, L., et al. (2022). Experimental study on morphology, nanostructure and oxidation reactivity of particles in diesel engine with exhaust gas recirculation (EGR) burned with different alternative fuels. *Energy* 261, 125249. doi:10.1016/j.energy.2022.125249

Huang, H., Tian, J., Li, J., and Tan, D. (2022). Effects of different exhaust gas recirculation (EGR) rates on combustion and emission characteristics of biodiesel-diesel blended fuel based on an improved chemical mechanism. *Energies* 15 (11), 4153. doi:10.3390/en15114153

Jayabal, R., Subramani, S., Dillikannan, D., Devarajan, Y., Thangavelu, L., Nedunchezhiyan, M., et al. (2022). Multi-objective optimization of performance and emission characteristics of a CRDI diesel engine fueled with sapota methyl ester/diesel blends. *Energy* 250, 123709. doi:10.1016/j.energy.2022.123709

Kim, T., Park, J., and Cho, H. (2020). Emission characteristics under diesel and biodiesel fueled compression ignition engine with various injector holes and EGR conditions. *Energies* 13 (11), 2973. doi:10.3390/en13112973

Krishnan, M. G., and Rajkumar, S. (2022). Effects of start of injection and exhaust gas recirculation on dual fuel combustion of isobutanol with diesel and waste cooking oil biodiesel in a diesel engine at higher loads. *Fuel* 327, 125097. doi:10.1016/j.fuel.2022.125097

Kumar, P. V., Ashok, B., Kumar, M. S., Vignesh, R., Bhasker, J. P., and Kumar, A. N. (2022). Evaluation of performance, emissions and combustion attributes of CI engine using palmyra biodiesel blend with distinct compression ratios, EGR rates and nano-particles. *Fuel* 321, 124092. doi:10.1016/j.fuel.2022.124092

Li, J., Han, Z., Shen, C., and Lee, C. F. (2014). Numerical study on the nitrogen oxide emissions of biodiesel-diesel blends in a light-duty diesel engine. *P I Mech. Eng. D-J Aut.* 228 (7), 734–746. doi:10.1177/0954407014521174

Li, X., Zhen, X., Wang, Y., Liu, D., and Tian, Z. (2019). The knock study of high compression ratio SI engine fueled with methanol in combination with different EGR rates. *Fuel* 257, 116098. doi:10.1016/j.fuel.2019.116098

Liang, J., Zhang, Q., Chen, Z., and Zheng, Z. (2021). The effects of EGR rates and ternary blends of biodiesel/n-pentanol/diesel on the combustion and emission characteristics of a CRDI diesel engine. *Fuel* 286, 119297. doi:10.1016/j.fuel.2020.119297

Mamat, R., Yusop, A. F., Abdullah, A. A., Aziz, A., and Abdullah, N. R. (2013). Effect of exhaust gas recirculation system and air temperature on exhaust emission of a diesel engine operating with biodiesel. *J. Biobased Mat. Bioenergy* 7 (4), 461–463. doi:10.1166/jbmb.2013.1346

Ozturk, E., and Can, O. (2022). Effects of EGR, injection retardation and ethanol addition on combustion, performance and emissions of a DI diesel engine fueled with canola biodiesel/diesel fuel blend. *Energy* 244, 123129. doi:10.1016/j.energy.2022.123129

Palani, Y., Devarajan, C., Manickam, D., and Thanikodi, S. (2022). Performance and emission characteristics of biodiesel-blend in diesel engine: A review. *Environ. Eng. Res.* 27 (1), 1–12. doi:10.4491/eer.2020.338

Ramadhas, A. S., Jayaraj, S., and Muraleedharan, C. (2010). Performance and emission studies on biodiesel-liquefied petroleum gas dual fuel engine with exhaust gas recirculation. *J. Renew. Sustain. Energy* 2 (1), 013109. doi:10.1063/1.3302019

Ramesh, T., Sathiyagnanam, A. P., De Poures, M. V., and Murugan, P. (2022). A comprehensive study on the effect of dimethyl carbonate oxygenate and EGR on emission reduction, combustion analysis, and performance enhancement of a CRDI diesel engine using a blend of diesel and prosopis juliflora biodiesel. *Int. J. Chem. Eng.* 2022, 5717362. doi:10.1155/2022/5717362

Rostampour, A., Shojaeefard, M. H., and Molaeimanesh, G. R. (2022). A comprehensive investigation of RANS and LES turbulence models for diesel spray modeling via experimental diesel schlieren imaging. *P I Mech. Eng. C-J Mec.* 236 (15), 8321–8337. doi:10.1177/09544062221084192

Shanmugam, S. K. M., Muthusamy, S., Ramasamy, R. K., and Alagumalai, A. (2022). Towards improved performance and lower exhaust emissions using exhaust gas recirculation coupled compression ignition engine fuelled with nanofuel blends. *ENERG SOURCE PART A*. doi:10.1080/15567036.2022.2038734

Shi, Z., Peng, Q., E, J., Xie, B., Wei, J., Yin, R., et al. (2023). Mechanism, performance and modification methods for NH_3-SCR catalysts: A review. *Fuel* 331, 125885. doi:10.1016/j.fuel.2022.125885

Tan, D., Chen, Z., Li, J., Luo, J., Yang, D., Cui, S., et al. (2021). Effects of swirl and boiling heat transfer on the performance enhancement and emission reduction for a medium diesel engine fueled with biodiesel. *Processes* 9 (3), 568. doi:10.3390/pr9030568

Tan, D., Meng, Y., Tian, J., Zhang, C., Zhang, Z., Yang, G., et al. (2023a). Utilization of renewable and sustainable diesel/methanol/n-butanol (DMB) blends for reducing the engine emissions in a diesel engine with different pre-injection strategies. *Energy* 269, 126785. doi:10.1016/j.energy.2023.126785

Tan, D., Wu, Y., Lv, J., Li, J., Ou, X., Meng, Y., et al. (2023b). Performance optimization of a diesel engine fueled with hydrogen/biodiesel with water addition based on the response surface methodology. *Energy* 263, 125869. doi:10.1016/j.energy.2022.125869

Venu, H., Subramani, L., and Raju, V. D. (2019). Emission reduction in a DI diesel engine using exhaust gas recirculation (EGR) of palm biodiesel blended with TiO_2 nano additives. *Renew. Energy* 140, 245–263. doi:10.1016/j.renene.2019.03.078

Wei, H., Zhao, W., Lu, Z., and Zhou, L. (2019). Effects of oxygen concentrations on the ignition and quasi-steady processes of n-heptane spray flames using large eddy simulation. *Fuel* 241, 786–801. doi:10.1016/j.fuel.2018.12.097

Wu, G., Ge, J., Kim, M. S., and Choi, N. J. (2022). NO_x-smoke trade-off characteristics in a palm oil-fueled CRDI diesel engine under various injection pressures and EGR rates. *Appl. Sci.-Basel* 12 (3), 1069. doi:10.3390/app12031069

Ye, J., E, J., and Peng, Q. (2023). Effects of porosity setting and multilayers of diesel particulate filter on the improvement of regeneration performance. *Energy* 263, 126063. doi:10.1016/j.energy.2022.126063

Yilbasi, Z., Yesilyurt, M. K., Yaman, H., and Arslan, M. (2022). The industrial-grade hemp (cannabis sativa L.) seed oil biodiesel application in a diesel engine: Combustion, harmful pollutants, and performance characteristics *Sci. Tech. Energy Transit.* 77, 15. doi:10.2516/stet/2022011

Yin, X., Li, W., Zhang, W., Lv, X., Yang, B., Wang, Y., et al. (2022). Experimental analysis of the EGR rate and temperature impact on combustion and emissions characteristics in a heavy-duty NG engine. *Fuel* 310, 122394. doi:10.1016/j.fuel.2021.122394

Yousefi, A., Guo, H., and Birouk, M. (2018). Effect of swirl ratio on NG/diesel dual-fuel combustion at low to high engine load conditions. *Appl. Energy* 229, 375–388. doi:10.1016/j.apenergy.2018.08.017

Zhang, B., Li, X., Wan, Q., Liu, B., Jia, G., and Yin, Z. (2023a). Hydrocarbon emission control of an adsorptive catalytic gasoline particulate filter during cold-start period of the gasoline engine. *Energy* 262, 125445. doi:10.1016/j.energy.2022.125445

Zhang, B., Li, X., Zuo, Q., Yin, Z., Zhang, J., Chen, W., et al. (2022a). Effects analysis on hydrocarbon light-off performance of a catalytic gasoline particulate filter during cold start. *Environ. Sci. Pollut. Res.* 29 (51), 76890–76906. doi:10.1007/s11356-022-20519-0

Zhang, Y., Zhong, Y., Lu, S., Zhang, Z., and Tan, D. (2022b). A comprehensive review of the properties, performance, combustion, and emissions of the diesel engine fueled with different generations of biodiesel. *Processes* 10 (6), 1178. doi:10.3390/pr10061178

Zhang, Z., Dong, R., Lan, G., Yuan, T., and Tan, D. (2023b). Diesel particulate filter regeneration mechanism of modern automobile engines and methods of reducing PM emissions: A review. *Environ. Sci. Pollut. Res.* 30, 39338–39376. doi:10.1007/s11356-023-25579-4

Zhang, Z., Dong, R., Tan, D., Duan, L., Jiang, F., Yao, X., et al. (2023c). Effect of structural parameters on diesel particulate filter trapping performance of heavy-duty diesel engines based on gray correlation analysis. *Energy* 271, 127025. doi:10.1016/j.energy.2023.127025

Zhang, Z., Li, J., Tian, J., Dong, R., Zou, Z., Gao, S., et al. (2022c). Performance, combustion and emission characteristics investigations on a diesel engine fueled with diesel/ethanol/n-butanol blends. *Energy* 249, 123733. doi:10.1016/j.energy.2022.123733

Zhang, Z., Lv, J., Li, W., Long, J., Wang, S., Tan, D., et al. (2022d). Performance and emission evaluation of a marine diesel engine fueled with natural gas ignited by biodiesel-diesel blended fuel. *Energy* 256, 124662. doi:10.1016/j.energy.2022.124662

Zhang, Z., Lv, J., Xie, G., Wang, S., Ye, Y., Huang, G., et al. (2022e). Effect of assisted hydrogen on combustion and emission characteristics of a diesel engine fueled with biodiesel. *Energy* 254, 124269. doi:10.1016/j.energy.2022.124269

Zhang, Z., Ye, J., Tan, D., Feng, Z., Luo, J., Tan, Y., et al. (2021). The effects of Fe_2O_3 based DOC and SCR catalyst on the combustion and emission characteristics of a diesel engine fueled with biodiesel. *Fuel* 290, 120039. doi:10.1016/j.fuel.2020.120039

Zhao, X., E, J., Liao, G., Zhang, F., Chen, J., and Deng, Y. (2021). Numerical simulation study on soot continuous regeneration combustion model of diesel particulate filter under exhaust gas heavy load. *Fuel* 290, 119795. doi:10.1016/j.fuel.2020.119795

Zhao, X., Jiang, J., Zuo, H., and Jia, G. (2023). Soot combustion characteristics of oxygen concentration and regeneration temperature effect on continuous pulsation regeneration in diesel particulate filter for heavy-duty truck. *Energy* 264, 126265. doi:10.1016/j.energy.2022.126265

Zhao, X., Zuo, H., and Jia, G. (2022). Effect analysis on pressure sensitivity performance of diesel particulate filter for heavy-duty truck diesel engine by the nonlinear soot regeneration combustion pressure model. *Energy* 257, 124766. doi:10.1016/j.energy.2022.124766

Zuo, H., Zhu, Y., Wu, S., Abubakar, S., and Li, Y. (2022). Effect of a crossed-semicircular-plate on thermal performance of micro-combustor fueled by premixed hydrogen-air mixture. *Int. J. Hydrogen Energy* 47 (39), 17442–17453. doi:10.1016/j.ijhydene.2022.03.2120360-3199